RGNZ/MGPB

The Integrated Analysis of Basement Faults in North Bangka Island, Indonesia, Using Surface Lineament Density and Gravity Anomaly Enhancement

Rudarsko-geološko-naftni zbornik
(The Mining-Geology-Petroleum Engineering Bulletin)
DOI: 10.17794/rgn.2026.2.15

Original scientific paper

Harnanti Yogaputri Hutami[1,2*], Edy Sunardi[1], Iyan Haryanto[1], Sonny Winardhi[3], Nugroho Prasetyo[2], Nur Ayu Anas[4], Erlangga Ibrahim Fattah[2]

[1] *Faculty of Geological Engineering, Universitas Padjajaran, Jln. Raya Bandung-Sumedang Km. 21, Jatinangor, 45363, Indonesia.*

[2] *Department of Geophysical Engineering, Faculty of Industrial Engineering, Institut Teknologi Sumatera (ITERA), Jln. Terusan Ryacudu, Jatiagung, Lampung Selatan, 35365, Indonesia.*

[3] *Department of Geophysical Engineering, Faculty of Mining and Petroleum Engineering, Institut Teknologi Bandung, Jln. Ganesha No. 10, Bandung, West Java, 40132, Indonesia.*

[4] *Geological Engineering Department, Faculty of Engineering, Cendrawasih University, Jln. Kamp Wolker, Papua, 99351, Indonesia.*

Abstract

Bangka Island was formed by the subduction and collision of the Gondwana-derived Sibumasu and East Malaya blocks in the Late Paleozoic. Its northern region comprises Permian metamorphic rocks of the Pemali Complex, Triassic sedimentary units from the Tanjunggenting Formation, and Late Triassic to Early Jurassic granites of the Klabat Formation. Despite multiple tectonic phases shaping Bangka Island, the structural configuration of basement faults and folds in the northern region remains poorly constrained. This uncertainty hampers the assessment of fractured basement reservoirs in the study area. To address this gap, this study integrates surface lineament extraction from DEMNAS with gravity anomaly data from GGMplus to investigate the basement structure of the northern Bangka. Fast Sigmoid Edge Detection (FSED) and Euler Deconvolution were applied to enhance structural interpretation and estimate basement depth. The dominant structural orientations of NW-SE and NE-SW identified at the surface were consistent with the subsurface features; however, FSED and Euler Deconvolution also revealed E-W and N-S trends. Moreover, the findings from the Euler Deconvolution indicated basement depths of 3000-4000 m below sea level. Field fracture measurements from granitic outcrops validate these orientations, confirming a strong correspondence between surface and subsurface structures. These findings offer new insight into the tectonic evolution of the northern region of Bangka Island and highlight fault orientations that may aid in identifying fractured basement reservoir zones in granitic terrains.

Keywords:
lineament density, enhanced edge detection, gravity anomaly, basement fault structures, Bangka Island

1. Introduction

Fractured basement reservoirs have emerged as significant hydrocarbon exploration targets, with important discoveries in Southeast Asia, such as the Bach Ho Field, Vietnam (**Areshev et al., 1992; Cuong & Warren, 2009; Hung et al., 2003; Hung & Le, 2004**) and the Suban gas Field, South Sumatra Basin, Indonesia (**Hennings et al., 2012; Koning et al., 2021; Kurniawan, 2018; Permana et al., 2023; Schultz, 2014**). These fields produce hydrocarbons from fractured granitic basement rock (**Cuong & Warren, 2009; Petford & McCaffrey, 2003**) and the reservoirs are strongly controlled by major fault systems that created interconnected fracture networks, allowing the fluid storage and migration (**Gutmanis, 2009; Guttormsen, 2010; Li et al., 2004**). Unlike conventional clastic and carbonate reservoirs, crystalline basement rocks (e.g. granite) are essentially non-porous and impermeable in their pristine state (**Narr et al., 2006; P'an, 1982**). As a result, their reservoir quality is almost entirely dependent on secondary porosity and permeability by brittle deformation, specifically through faults, shear zones, and fracture networks (**Gillespie et al., 2018; Gillespie et al., 2021; Guttormsen, 2010; Suyoto, 2010; Tjia, 2007**). While carbonates may also function as fracture-controlled reservoirs, they often benefit from additional enhancement through chemical dissolution and karstification, which is absent in crystalline rocks. However, this makes tectonic setting and structural analysis especially critical in assessing the potential of basement reservoirs.

Given the significance of such structurally controlled basement reservoirs in Southeast Asia, attention also turns to Bangka Island, which lies off the east coast of South Sumatra. The island, with a land area of 11,500 km^2,

* Corresponding author: Harnanti Yogaputri Hutami
e-mail address: harnanti.hutami@tg.itera.ac.id
Received: 4 June 2025. Accepted: 1 November 2025.
Available online: 13 March 2026

forms part of the Sundaland continental crust, shaped by long-lived and complex tectonic processes (**Hall et al., 2009; Katili, 1972; Metcalfe, 2017; Van Gorsel, 2018**). Its geology comprises Permo-Carboniferous metamorphic and Triassic sedimentary sequences, intruded by Late Triassic to Jurassic granitic bodies. However, detailed structural studies have been limited by tropical weathering, dense vegetation, and poor outcrop conditions (**Katili, 1967; Ko, 1986**). Earlier surface investigation from **Ko (1986)** provided only a preliminary overview, and despite centuries of tin mining, systematic studies of basement faults remain scarce. Consequently, the structural configuration of Bangka's basement and its implications for fractured reservoir potential remain poorly constrained. To address this gap, this study integrates surface lineament mapping with edge-detected gravity anomalies analysis derived from satellite data to characterise the structural pattern and orientation of Bangka's granitic basement.

Lineaments, expressed as linear features such as faults, folds, or fracture zones, provide a surface manifestation of underlying tectonic structures (**Ahmadi & Pekkan, 2021; Hung et al., 2005**). The term 'lineament' was first introduced by **Hobbs (1904),** who characterised it as a significant linear landscape that exposes the underlying architecture of a distinct rock basement. Their systematic mapping improves understanding of tectonic and structurally controlled reservoirs (**Army & Saepuloh, 2020; Enoh et al., 2021; Florinsky, 2016; Mohammed et al., 2010**). Satellite-derived datasets, such as the National Digital Elevation Model (DEMNAS), allow the systematic extraction of surface lineaments in the observation area (**Han et al., 2018; Prabowo et al., 2021**). To complement surface analysis, gravity anomaly data offered insight into subsurface structures. The enhancement techniques play an essential role in detecting boundaries of geological formations and understanding the structural setting (**Eldosouky et al., 2022; Kumar & Singh, 2021; Kumar et al., 2018; Melouah & Pham, 2021**). In this study, we applied an enhanced edge detection filter, known as Fast Sigmoid Edge Detection Filter (FSED), based on a modified fast sigmoid function and the vertical and horizontal derivatives of the total horizontal gradient of gravity data, as proposed by **Oksum et al. (2021)**. This edge detection filter provides maximum amplitudes on the edges of the anomalous sources and simultaneously balances anomalies from deep and shallow geological sources, as proven by several previous tectonic and structural studies (**Aprina et al., 2024; Liu et al., 2023; Pham et al., 2021; Safani et al., 2023**).

Research into the tectonic and structural geology of Bangka Island has applied diverse approaches, including petrographic, geochemical, and geophysical methods. Petrographic studies revealed granitoids dominated by alkali feldspar-syenogranite, while geochemical data indicated a calc-alkalic magma affinity, consistent with a subduction-collision origin characteristics (**Widana, 2013**). Structural investigations further support this interpretation. **Hendrawan et al. (2024)** documented three main deformation phases, involving folding and faulting, and emphasized the presence of complex metamorphic structures in northern Bangka that related to block collision. Remote sensing had also provided insights into the tectonic framework. Shuttle Radar Topography Mission (SRTM) data highlighted dominant NW-SE and NE-SW lineament orientations, reflecting significant tectonic deformation (**Franto, 2015**). Moreover, major NE-SW trending structures, namely Pemali and Payung faults, exerted a strong influence on the regional radiogenic geothermal system and geological formations in the area (**Siregar et al., 2024**). These studies demonstrated the polyphased tectonic history of Bangka Island. However, the geometry and continuity of basement structures remain poorly understood, underscoring the need for integrated surface and subsurface structural analysis.

The present study provides a comprehensive structural analysis of the Paleozoic-Mesozoic granitic basement in the northern part of Bangka Island by integrating surface lineament mapping with edge-detected gravity anomalies. The objective is to correlate surface and subsurface structures to better constrain the geometry and continuity of basement features and assess their implications for regional tectonic evolution and the potential for fractured reservoirs. Furthermore, natural fracture measurements from granite outcrops were included in the study to validate the integrated analysis, providing important field-based properties to support the structural interpretations.

2. Geological setting

The geology of Bangka Island is characterized by two different settings: (1) northern Bangka (**Mangga & Djamal, 1994**), dominated by the Permian Pemali Complex; and (2) southern Bangka, characterized by the Triassic Tanjung Genting Formation and Jurassic granite (**Margono et al., 1995**). The granite on Bangka Island was formed as a result of the subduction and collision of the East Malaya Block and the Sibumasu Block (**Cobbing et al., 1986; Hutchison, 2014; McCourt et al., 1996; Metcalfe, 2000, 2017**). Field observation through geochemical and petrographic studies (**Widana, 2013**) supported the information. **Figure 1** shows the geology map of the northern Bangka, modified after **Mangga & Djamal (1994)** and **Ko (1986)**. The map illustrates the distribution of the main lithological units, including Permian Pemali Complex (CPp), the Triassic Tanjunggenting Formation (TRt), and the Late Triassic-Jurassic Klabat Granite (TRJkg), along with the Tertiary Ranggam Formation (TQr), Penyabung Diabase (PTrd), and Quaternary alluvium deposits (Qa). This map was complemented by an NW-SE cross-section (line A-A') that

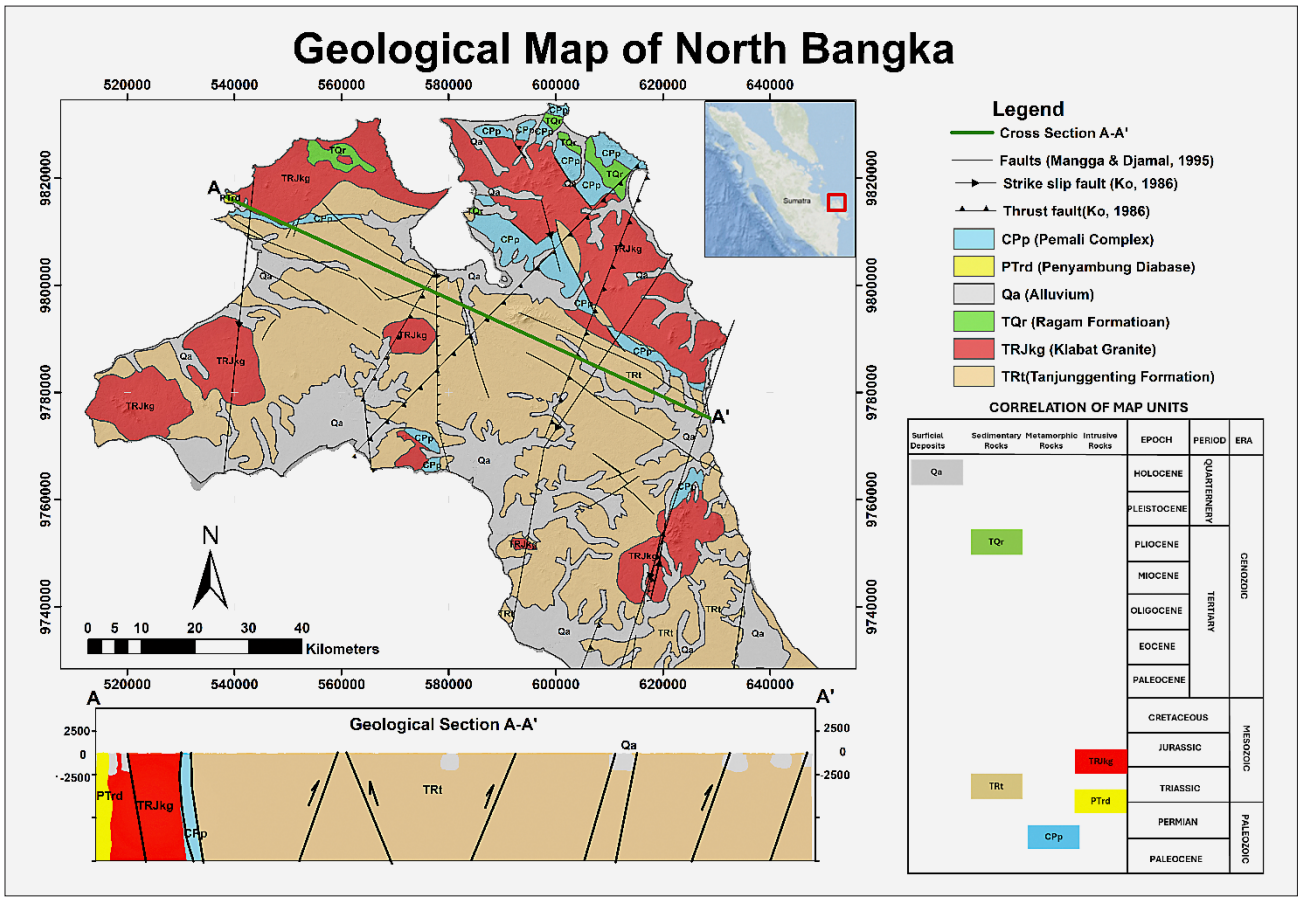

Figure 1. Map of the northern region of Bangka Island with the NW-SE-oriented subsurface model (line A-A'), modified after **Mangga & Djamal (1994)** and **Ko (1986)**.

depicted the stratigraphic relationships between the rock units, the granite intrusions, and associated faults, which represented the block faulting systems in the study area.

The northern region of the island comprised two principal basement sequences: the Pemali Complex consisted of deep marine cherts, black shales, and volcaniclastic sediments deposited in a subsiding continental slope environment, formed on the Paleotethys floor and later incorporated into the accretionary complex during the collision of the Sibumasu Block and the east Malaya Block in the Late Permian (**Barber et al., 2005; Metcalfe, 2013, 2017**). In the Early Triassic, subsidence occurred, and the Tanjung Genting Formation was deposited in the shallow marine environment. This formation unconformably overlies the Pemali Complex and comprises alternating meta-sandstones, sandstones, clayey sandstone, and claystone with oxide limestone. The Tanjung Genting Formation was subsequently folded and locally thrust over the older units, likely linked to Late Triassic tectonism and the granitic intrusion events of the Klabat granite (**Ko, 1986**), which consists of biotite granite, granodiorite, and gneissic granite. These stratigraphic relationships are supported by radiometric data and biostratigraphy, which place the granitoid intrusions near the Norian-Rhaetian boundary (~ 214 – 217 Ma), as confirmed by Sr isotopic studies by **Ng et al. (2017)**.

The tectonic evolution of northern Bangka was marked by at least three deformation phases (**Mangga & Djamal, 1994**): (i) Late Paleozoic NE-SW trending structures, (ii) Triassic-Jurassic NW-SE trending faults and folds, likely linked to the old ocean suture of the Bentong-Raub Line that intersected in the east of Bangka Island (**Ng et al., 2017**), and (iii) Cretaceous N-S faulting (**Franto, 2015**). These multiphase structures strongly influenced the development of fracture systems within the basement rocks. Their identification and validation through surface measurements of natural fractures provide a critical link to understand the study area's tectonic history and assess the fractured basement reservoir potential.

3. Methods

3.1. Data

This study employed a combination of satellite-derived and geophysical datasets to conduct analyses of subsurface structures in the northern region of Bangka Island, Indonesia. The topographic data were sourced from the Digital Elevation Model Nasional (DEMNAS), an official product provided by Indonesia's Badan Informasi Geospasial (BIG). DEMNAS integrates elevation

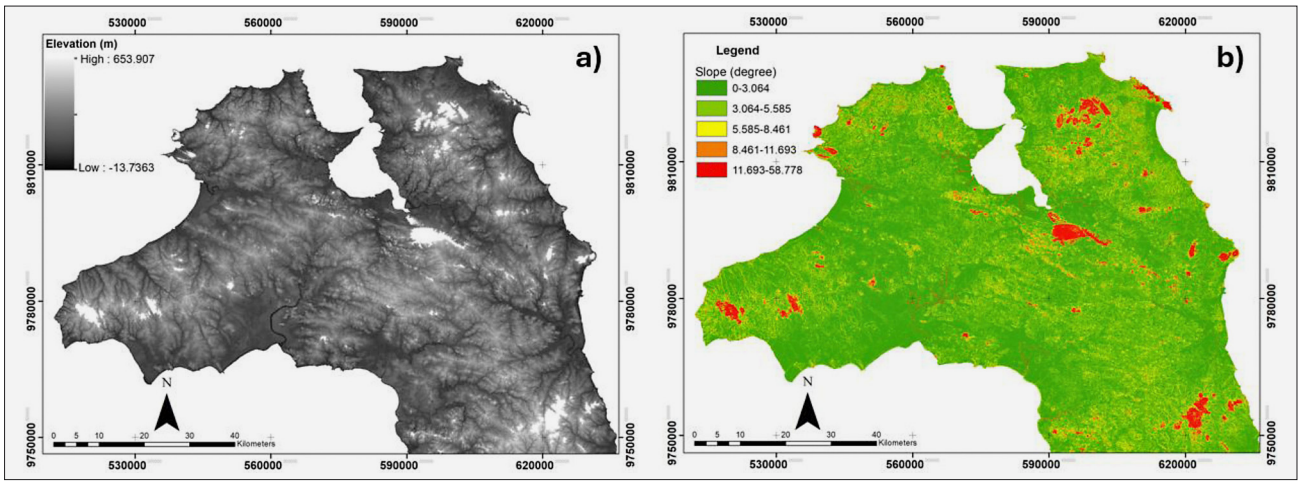

Figure 2. a) DEMNAS input for lineament extraction with a spatial resolution of 8,1 m; b) slope model of the study area

data from multiple sources, including Interferometric Synthetic Aperture Radar (IFSAR) and TerraSAR-X, achieving a high spatial resolution of approximately 8.1 meters (0.27 arc-seconds). This degree of detail is particularly advantageous for detailed geomorphological and structural mapping (see **Figure 2a**). As illustrated in **Figure 2b**, the study area is generally characterized by low-relief morphology, with most of the terrain gently undulating and the highest elevations at 653 meters. Although local hills and ridges are present in association with granitic intrusions and fault-controlled structures, the steepest slope measures approximately 58 degrees. Given these topographic characteristics, the lineaments were semi-automatically digitized from enhanced raster layers, ensuring topographic continuity, alignment with geomorphological features, and geological plausibility.

For subsurface delineation using the FSED technique, we utilized high-resolution satellite gravity data from the Gravity Model Plus 2013 (GGMplus 2013), developed by **Hirt et al. (2013)**, to delineate geological structure patterns and their associated tectonic settings. The GGMPlus model integrates GOCE/GRACE satellite gravity, Earth gravity models (EGM2008), and topographical gravity derived from SRTM topography (**Hirt, 2014; Hirt et al., 2013**). These data provide a spatial resolution of approximately 200 m (~ 7.2 arc-seconds) over both land and marine areas. A gravity anomaly grid covering the Bangka Island region was extracted in GeoTIFF format, projected to WGS 1984 UTM Zone 48S, and resampled to match the spatial resolution of DEMNAS for seamless integration. Free-air gravity anomalies were used to retain structural signals associated with density contrasts in the subsurface granitic basement. Subsequently, several gravity corrections were applied to generate the Complete Bouguer Anomaly (CBA) map covering Bangka Island, which was then utilized as input for residual anomaly analysis and enhanced edge detection techniques.

3.2. *Lineament extraction process*

The lineament extraction process employed a semi-automated methodology, which required subsequent manual refinements to enhance the accuracy of the extracted lineaments. This approach ensures that the digitized linear features faithfully represent the geological characteristics observed (**Carvalho & Batty, 2005**). This extraction is based on the precise detection of line segments within the imagery (**Azman et al., 2020**). In the preliminary phase, we carefully adjusted various parameters to enhance the accuracy of the extraction results. This optimization process ensured optimal extraction results.

Table 1. List of adjusted parameters utilized in the data input for lineament extraction

No.	Parameter	Value
1	RADI (*Filter Radius*)	10
2	GHTR (*Gradient Threshold*)	100
3	LTHR (*Length Threshold*)	30
4	FTHR (*Line Fitting Error Treshold*)	3
5	ATHR (*Angular Difference Threshold*)	30
6	DTHR (*Linking Distance Threshold*)	20

The raster mosaicking process integrates multiple sections of DEMNAS data from the study area into a cohesive raster format. We produced a hillshade digital elevation model (DEM) image that visually depicts the terrain by simulating the effects of light on the surface. This method effectively emphasizes the area's relief and topographic variations. Our primary objective was to illustrate these variations through light and shadow, tailored to a specified direction of incoming sunlight. By utilizing the shadow effects created by this sunlight, we provided a clear representation of the area's relief and topographic features (**Farmakis-Serebryakova & Hurni, 2020; Rusinkiewicz et al., 2006**). An azimuth angle

and a solar elevation angle of 45 degrees were employed to determine the optimal lighting direction and evaluate the resulting shadow intensity. The results provided a comprehensive and informative representation of the morphological features within the study area, including slopes, ridges, and valleys.

The extracted lineaments were manually corrected in subsequent steps to ensure that the digitized linear features accurately represent the geological characteristics. This extraction relied on detecting linear segments within the imagery (**Ni et al., 2016**). During this process, various parameters were systematically adjusted to enhance the accuracy of the extraction results (refer to **Table 1**). Each parameter utilized in the extraction process was essential for three primary stages: edge detection, threshold determination, and curve extraction (**Bampourda et al., 2017**). These stages involved a series of complex processes that ensured the extracted lineaments were accurate and aligned with the observed geological conditions (**Salui, 2018**).

The initial edge detection stage employs the Canny edge detection algorithm, which generates an edge strength image that underlies the lineament extraction process. This algorithm consists of three systematic steps: (1) *Filtering* - the input image is processed through a Gaussian function (**Bhardwaj et al., 2020**), with the radius determined by the RADI parameter. This step is designed to smooth the image and minimize noise, thereby enhancing the effectiveness of the edge detection process, (2) *Gradient Calculation*–the gradient of the filtered image is computed to detect intensity changes that signify the presence of edges–and (3) *Non-Maximum Suppression* - pixels that do not represent local maxima in the gradient are suppressed by assigning them an edge strength of zero (**Vincent & Folorunso, 2009**). This method ensures the preservation of only the most significant edges for analysis in subsequent stages.

In the second stage of the process, the edge-detected image is further refined by applying a threshold, which produces a binary image. In this binary representation, each ON pixel represents a detected edge element. The thresholding operation is controlled by the GTHR (Edge Gradient Threshold) parameter (**Ng, 2006**), which specifies the minimum edge intensity for inclusion in the extraction. Applyin this threshold ensures that only edge features meeting predefined criteria are retained, while less significant elements are excluded.

In the third stage, the curve extraction process uses the binary edge image generated in the preceding step. This stage encompasses several critical sub-steps to accurately represent the extracted linear features. A thinning algorithm is initially applied to the binary image, transforming the edge elements into one-pixel-wide skeleton curves. Subsequently, each curve is extracted as a series of pixels. To enhance the efficiency of the extraction process, a filtering mechanism is employed to eliminate curves that do not meet the established Curve Length Threshold (LTHR). Curves falling below this threshold are regarded as insignificant for lineament analysis.

Upon completing the curve extraction process, the subsequent step involves converting the pixel curves into vector form by fitting line segments. This process generates a polygonal line that accurately represents the original curve, with the maximum error rate determined by the FTHR (Line Fitting Threshold) parameter. This methodology ensures that the resulting polygonal line closely adheres to the shape of the detected lineament.

In the final stage, the algorithm connects polyline pairs that meet the established criteria. The interconnection of two polylines occurs if the following conditions are met: (1) the terminal segments of each polyline must be oriented toward each other with consistent alignment, with the angle between them being less than the threshold set by the ATHR (Angular Threshold), and (2) the endpoints of the two polylines must be within proximity, with the distance between them being below the DTHR (Distance Threshold) value.

Through this comprehensive process, the system enhances the precision of lineament extraction, ensuring that the detected linear structures accurately represent the geological features at the Earth's surface (**Ahmadi & Pekkan, 2021; Echeverria et al., 2022; Enoh et al., 2021; Salui, 2018**). Finally, a comprehensive analysis of high-density lineament zones was conducted to identify areas of fracturing and rock cutting, as well as regions of greater deformation intensity, which correspond to the deformation phases observed in the study area.

3.3. Fast-Sigmoid Edge Detection (FSED) and Euler Deconvolution Procedures

The Fast-Sigmoid Edge Detection Filter (FSED) was applied to the enhanced gravity anomaly map to delineate structural boundaries and fracture zones (**Oksum et al., 2021; Pham, 2024; Pham et al., 2021**). A recent study using FSED effectively migrates amplitude anomalies arising from causative bodies at varying depths and with distinct properties, enhancing resolution and accuracy in delineating source edges. Notably, this filter avoids generating spurious edges when anomaly sources exhibit opposing density contrasts simultaneously (**Kamto et al., 2023; Oksum et al., 2021; Pham et al., 2021**), and it mitigates noise interference, ensuring superior edge detection quality in potential field data (**Li et al., 2014**). Therefore, edge enhancement techniques have feartly improved the accurate mapping of geological features, including faults, contacts, and dikes, providing critical insights into subsurface structures.

Several preparatory steps are essential before initiating the edge detection procedure using the FSED technique. The first step involves applying an average gravity value of 2.67 g/cm³ to generate a Complete Bouguer Anomaly (CBA) map of the target area. The subsequent

step is to perform a power spectrum analysis to estimate the width and depth of the gravity anomalies within the study area. This analysis also facilitates a comparison of the response spectra of various filtering methods. The power spectrum analysis was conducted utilizing the principles of the Fourier transform applied to horizontal plane gravity anomalies (**Blakely, 1995**).

To effectively separate residual anomalies from regional anomalies and achieve optimal window width estimation, we applied a logarithmic transformation to the amplitude spectrum obtained from the Fourier transform (refer to **Equation 1**). This transformation yielded a straight-line equation, facilitating clearer analysis and interpretation of the data.

$$\ln P = (z_0 - z)|k| \quad (1)$$

The equation illustrates that the component is directly proportional to the amplitude spectrum. Additionally, the linear regression applied to this equation helps to delineate the boundary between the first-order (regional zone) and the second-order (residual zone) zones. The value at this boundary is identified as the determinant of the window width. Moreover, the relationship between wavelength and amplitude is derived from **Equation 2**, which determines the window width (**Blakely, 1995**).

$$k = \frac{2\pi}{\lambda};\ \lambda = n \cdot \Delta x \quad (2)$$

Enhancement techniques play a crucial role in identifying the boundaries of geological formations and understanding their structural settings (**Eldosouky et al., 2022; Kumar et al., 2018; Ma et al., 2014; Melouah & Pham, 2021; Nasuti et al., 2019**). Edge detection methodologies are essential for interpreting potential field data, as they form the foundation for delineating geological structures and identifying subsurface discontinuities (**Liu et al., 2023; Pham, 2024**). Conventional edge detection filters typically rely on the computation of horizontal and vertical derivatives of potential field data or various combinations of these derivatives to accentuate regions of rapid change that signify structural boundaries (**Kamto et al., 2023; Yao et al., 2016**).

This nonlinear transformation function utilizes the sigmoid function to sharpen edge contrasts while suppressing background noise. It offers flexible and robust tools for enhancing subtle gravity gradients. The FSED equation (**Oksum et al., 2021**) is expressed in **Equations 3** and **4** as follows:

$$\mathrm{FSED} = \frac{\mathrm{R} - 1}{1 + |\mathrm{R}|} \quad (3)$$

$$R = \frac{\frac{\partial \mathrm{THG}}{\partial \mathrm{z}}}{\sqrt{\left(\frac{\partial \mathrm{THG}}{\partial \mathrm{x}}\right)^2 + \left(\frac{\partial \mathrm{THG}}{\partial \mathrm{y}}\right)^2}} \quad (4)$$

where ∂THG/∂z - vertical derivative of the total horizontal gradient (THG); ∂THG/∂x - horizontal derivative of the total horizontal gradient in the X direction, and; ∂THG/∂y - horizontal derivative of the total horizontal gradient in the Y direction.

Finally, the basement depth information was acquired through the Euler Deconvolution analysis, as formulated in **Equation 5**.

$$(\mathrm{x} - \mathrm{x}_0)\frac{\partial^2 \mathrm{f}}{\partial \mathrm{x}^2} + (\mathrm{y} - \mathrm{y}_0)\frac{\partial^2 \mathrm{f}}{\partial \mathrm{y}^2} + (\mathrm{z} - \mathrm{z}_0)\frac{\partial^2 \mathrm{f}}{\partial \mathrm{z}^2} = \mathrm{N}\frac{\partial \mathrm{f}}{\partial \mathrm{z}} \quad (5)$$

Although this method was first implemented to determine the positions of lineaments in magnetic data (**Cooper, 2008**). Its employment in the gravity data has been widely acknowledged (**Eldosouky et al., 2022; Ghosh, 2022; Pham et al., 2024; Reid et al., 2003; Safani et al., 2023; Sembiring et al., 2023; Soleha et al., 2019**). The *f* denotes the gravity field at the point of *x,y,z* affected by the anomaly sources at x_0,y_0,z_0 position. The parameter N is defined as the sum of the structural index (SI) and the vertical gradient order of the gravity data (*n*). This value represents the structural index that characterises the geometric parameters of the source (**Cooper, 2008; Melo & Barbosa, 2018; Pham et al., 2024; Reid et al., 2003, 2012**). In the gravity data, SI = -1 represents a lithological contact or fault, 0 is for a thin sheet, 1 is used for a horizontal cylinder, and 2 is the geometric sphere (**Ghosh, 2022; Pham et al., 2024; Safani et al., 2023; Soleha et al., 2019**).

4. Results and Analysis

4.1. Lineament density analysis

The results of the lineament extraction conducted in the study area reveal specific lineaments most closely associated with geological features. A total of 1,266 lineaments were successfully identified, comprising 348 in the granitic Klabat Formation (TRJkg), 287 in the metamorphic Pemali Formation (CPp), 539 in the sedimentary Tanjung Genting Formation (TRt), 79 in the Ranggam Formation (TQr), and 13 in the Diabas Penyabung Formation (PTrd). To facilitate further analysis, the orientation of the lineaments in each formation is illustrated in a rose diagram, as shown in **Figure 3**.

The lineaments observed across the study area predominantly exhibit a northwest-southeast (NW-SE) orientation, which indicates a significant geological structure aligned in this direction. Furthermore, certain formations display additional, less prominent directional trends. For instance, the Quaternary-aged Ranggam Formation (TQr) reveals a north-south (N-S) orientation. At the same time, the Permo-Carboniferous-aged Diabas Penyabung Formation (PTrd) exhibits a northeast-southwest (NE-SW) orientation. A relative east-west (E-W) alignment is also present within the Triassic-Jurassic age formations. Overall, the detected lineament orientations correspond to the structural direction interpreted by **Mangga & Djamal (1994)** on their geological map of North Bangka.

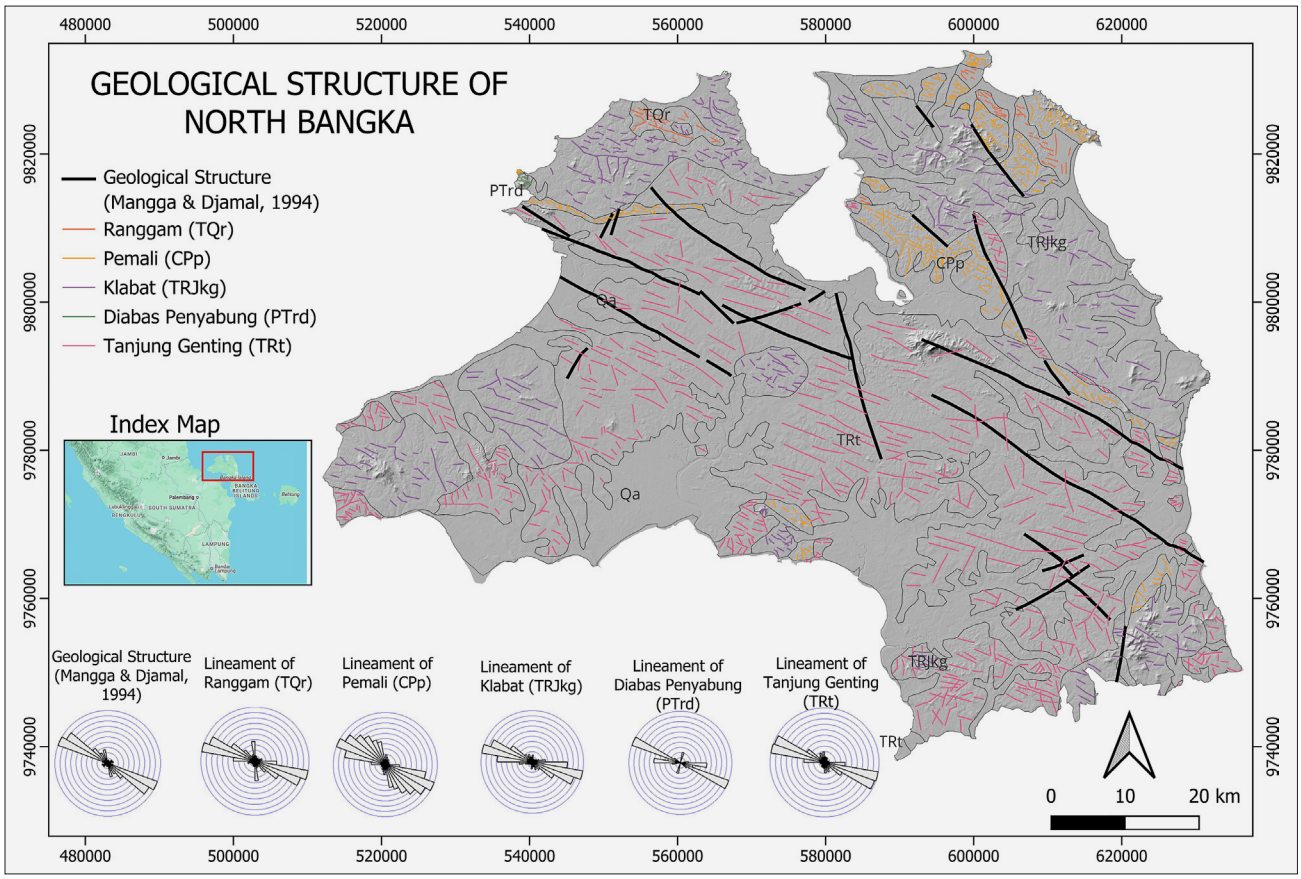

Figure 3. The extracted lineament in northern Bangka Island, Indonesia

Upon analyzing the primary directions of the identified surface lineaments, the next phase involves assessing their density. **Figure 4** illustrates the lineament density map of the study area across various geological formations, highlighting the specific intensity and distribution of structural deformation in relation to lithological characteristics. In this context, lineament length density quantifies the total lineament length per unit area (km/km²), directly indicating the deformation of rocks in response to regional tectonic stress, particularly through the development of fault and fold systems. The spatial distribution of lineament density, as depicted in the figure, shows significant alignment with major geological structures, particularly fault systems oriented in the northwest-southeast (NW-SE) and northeast-southwest (NE-SW) directions. These fault systems are integral to the regional Sumatra Fault pattern and its local branches in northern Bangka. High-density zones frequently coincide with or are parallel to the orientations of these prominent faults, suggesting that the lineaments are manifestations of fracture zones and fold planes resulting from tectonic stress.

A detailed analysis of each rock formation is outlined as follows:

1. **The Pemali Formation (CPp)** comprises Permo-Carboniferous metamorphic rocks, primarily phyllite. Within this formation, high lineament densities, reaching up to 0.70 km/km², are particularly evident in the northern and eastern regions. The phyllite is characterized by its parallel foliation planes, which are prone to fracturing along the foliation or schistosity zones. The dominant lineaments are aligned with fold axes and minor faults that have formed due to regional deformation.
2. **Penyabung Diabase Formation (PTRd)**, an intermediate intrusive body of Permian age, displays the highest lineament density of 10.33 km/km² within a limited geographical area. This elevated lineament occurrence is likely attributable to fault structures at the intrusion's margins. Furthermore, the extremely high density is also influenced by the small spatial extent of the body, which significantly increases the length-to-area ratio.
3. **Ragam Formation (TQr)**, composed of sandstone and clastic sediments from the Late Miocene, exhibits a maximum lineament density of 0.58 km/km², suggesting limited influence of regional structures. The highest density values are found in the northwest, while lower densities are observed in the northeast. Although sandstone can preserve fractures, it is less homogeneous compared to igneous or metamorphic rocks. Local folds and faults may generate minor lineaments within this formation.

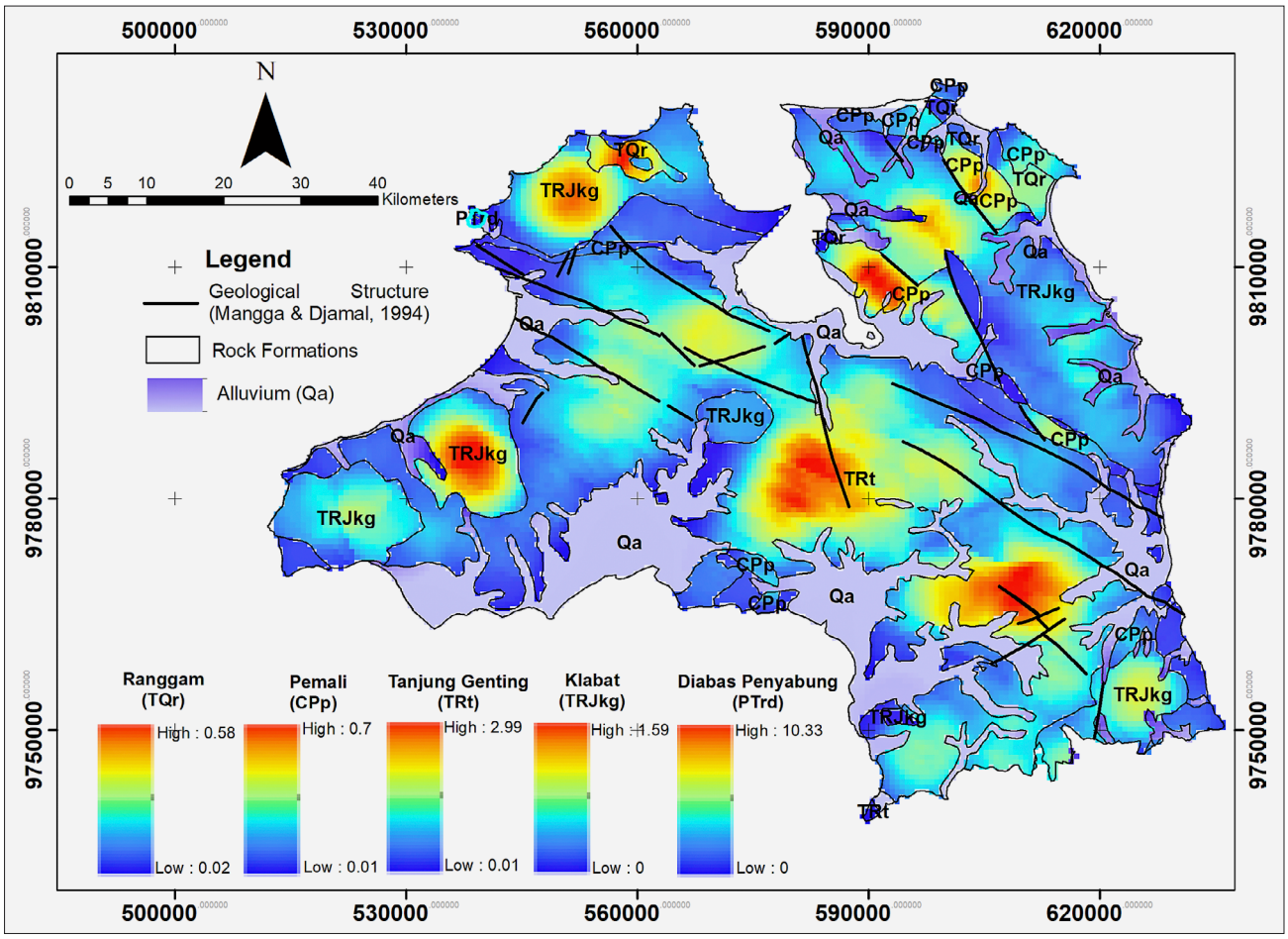

Figure 4. The lineament density map from the formation in the study area

4. **Klabat Granite Formation (TRJkg).** This formation comprises felsic granitoids from the Late Triassic to Jurassic periods. This unit demonstrates relatively high lineament densities, reaching up to 1.59 km/km², particularly in the western and northeastern regions. Due to its hardness, granite is highly susceptible to external stress, resulting in the development of fracture systems and sheet joints. These features manifest as lineaments and are frequently associated with major fault systems.
5. **Tanjung Genting Formation (TRt)**, composed of Triassic sandstones and clastic sediments, exhibits high lineament densities reaching up to 2.99 km/km². This phenomenon can be attributed to the presence of relatively hard rock material within the fault and folding zones of the formation. The alignment of the lineaments predominantly follows a northeast-southwest (NE–SW) direction.

The findings reveal that areas with high lineament density consistently align with major geological structures, indicating that lineaments effectively indicate fault and fold systems in northern Bangka. Variations in density values across different geological formations underscore the importance of conducting lithology-specific lineament analyses rather than relying on broad, regional generalizations, which can lead to interpretive inaccuracies. This formation-based analysis successfully captures the deformation intensity and orientation variability influenced by the region's principal fault and fold systems. Such an approach facilitates the identification of specific deformation zones and provides valuable insights into the mechanical behavior of each lithology under tectonic stress. The strong correlation between lineament density and major geological structures further underscores the utility of lineaments as a crucial tool for structural geological interpretation within the framework of regional tectonics.

4.2. Basement faults interpretation from FSED and Euler Deconvolution

The geological complexities of this region have resulted in a varied distribution of rocks and subsurface structures, significantly impacting the gravity field response. The Complete Bouguer Anomaly (CBA) map, presented in **Figure 5a**, delineates regional variations, with positive gravity anomaly values ranging from 16 to 38 mGal. The areas exhibiting the highest values, depicted in red to violet colours in the western region, reach a maximum of 38 mGal. This phenomenon indicates a greater topographic elevation and the presence of

denser rock types, such as granite intrusions. Conversely, the eastern region displays lower gravity anomaly values, represented by yellow to blue colors, which signify reduced density contrast relative to the surrounding geological structures. These lower gravity anomaly values suggest the presence of rock formations that originated during the Palaeozoic-Mesozoic era, which continue to undergo significant erosion and denudation processes.

The depth estimation of the anomaly source in this study utilizes the Radially Averaged Power Spectrum (RAPS) analysis, adapted from the work of (**Spector & Grant, 1970**). The average power spectrum's slope indicates the depth of discontinuity between two distinct anomalous sources. The segment of the curve with the lowest wavenumber values, ranging from 0 to 0.02 cycles/km, corresponds to deep anomalous sources. In contrast, wavenumbers exceeding 0.2 cycles/km are interpreted as signals from shallow anomalies, which may be classified as noise. Wavenumber values in the intermediate range of 0.02 to 0.2 cycles/km represent anomalies from geological features at intermediate depths. The boundaries of these depth segments for the anomalous sources are illustrated in **Figure 5b**. Following the anomaly separation process, the resulting residual gravity anomaly displays variations between -3 and 2 mGal, indicating the presence of shallower geological features, as shown in **Figure 5c**, specifically referring to the residual anomalies.

The geological characteristics in this study were further enhanced using the FSED technique, which produces values ranging from -1 to 1, as illustrated in **Figure 6a**. Additionally, the estimated depths derived from Euler Deconvolution, as shown in **Figure 6b**, are represented by colored dots distributed across the area, indicating the different depths of geological features that extend up to 3700 meters beneath the surface. The combination of these techniques enables the interpretation of the targeted geological features at the boundary where the value is maximum (**Kamto et al., 2023; Oksum et al., 2021; Pham et al., 2023**), as well as their estimated depths.

The analysis of geological structures utilizing the FSED approach indicates a clear predominance of orientations ranging from northwest-southeast (NW-SE) to north-south (N-S). Furthermore, geological features aligned in the east-west (E-W) direction were also observed as minor orientations. These directional variations are consistent with the geological features identified at the surface through lineament and lineament density analysis. Consequently, the structural features identified using the FSED method applied to gravity anomaly data corroborate the surface observations and suggest vertical continuity of these geological structures.

The analysis of depth estimates through Euler Deconvolution indicates that the identified gravity anomalies, corresponding to structural features, extend to depths of

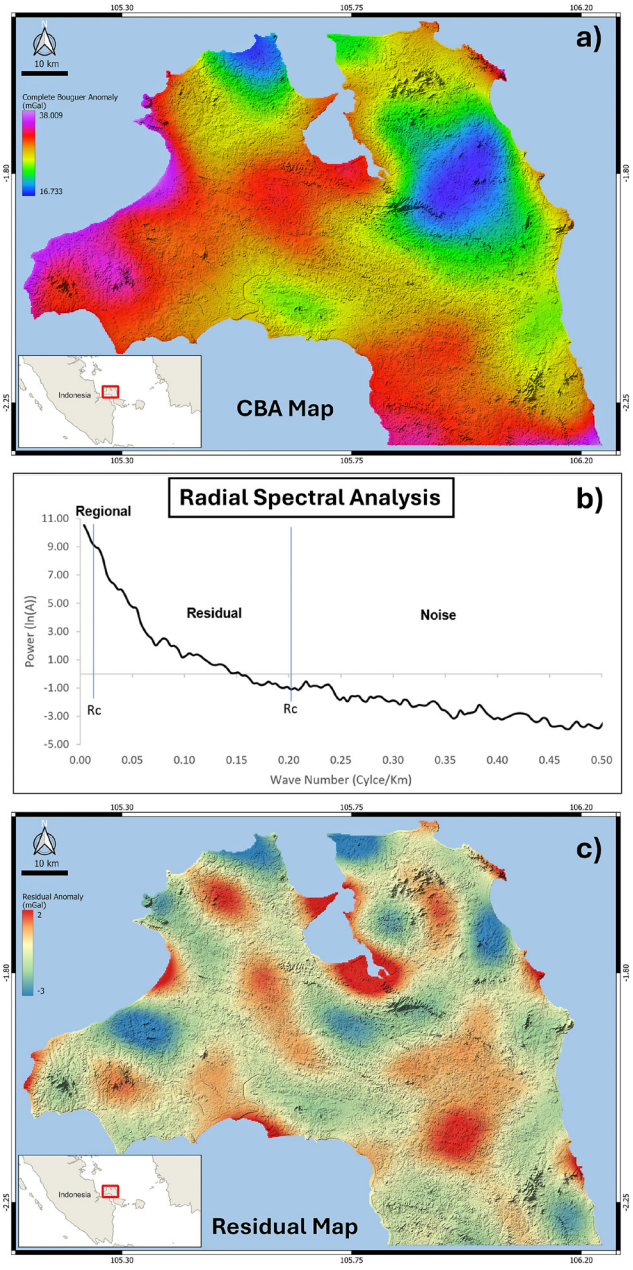

Figure 5. a) Complete Bouguer Anomaly (CBA) map, **b)** radial average power spectrum curve graph CBA data, and **c)** residual map of the study area

3000-4000 meters below sea level. These anomalies exhibit orientations that are consistent with those derived from FSED and surface lineament techniques. The primary structures observed from the Euler Deconvolution analysis are oriented in two predominant directions: northwest-southeast (NW-SE) and east-west (E-W). The NW-SE orientation displays a strong correlation with the second deformation phase associated with the Bentong-Raub thrust line, which extends across the eastern segment of the study area. Conversely, the E-W orientation is linked to thrust faults affecting the Tanjung Genting Formation (TRt) and has played a significant role in the formation of granitic plutons that intruded into the overlying formations in a similar directional pattern.

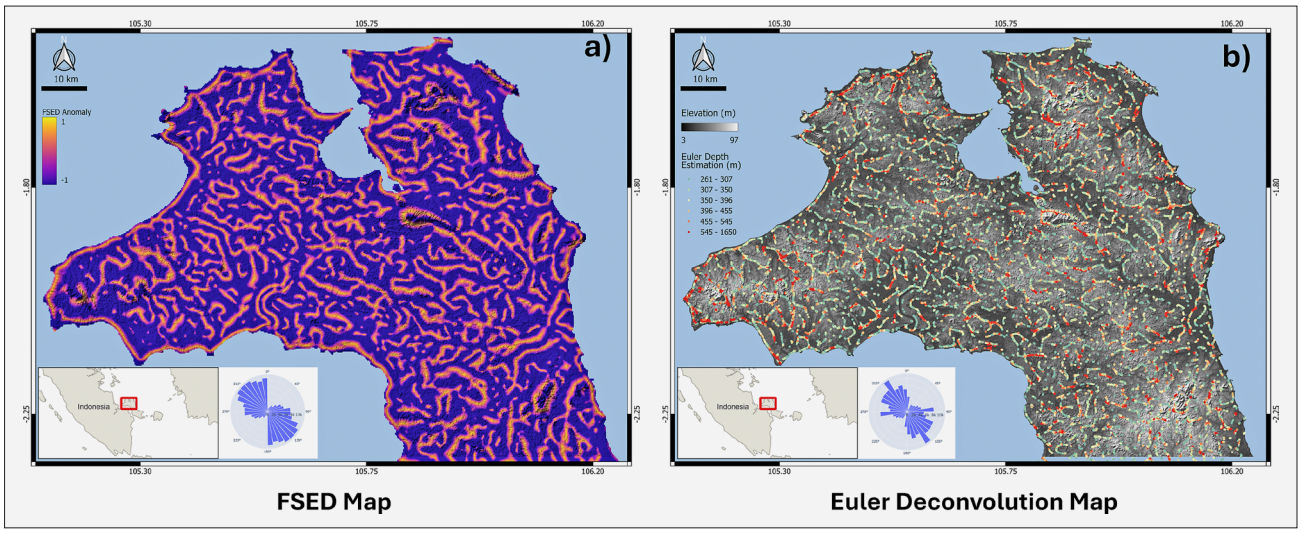

Figure 6. a) Subsurface structural lineaments from FSED and **b)** the estimated depth of structural lineaments from Euler Deconvolution

In addition to these two primary orientations, a minor northeast-southwest (NE-SW) direction, detected through both FSED and Euler Deconvolution, is interpreted as representing the initial deformation phase from the Palaeozoic era. The subduction and collision of the Sibumasu and East Malaya microplates characterise this phase. Furthermore, the north-south (N-S) direction is regarded as the most recently formed minor structure, intersecting older formations in the study area. Its formation is likely influenced by tectonic activity originating from Sumatra that extends to the northern region of Bangka Island and manifests as regional shear faults with similar orientation (**Barber et al., 2005; Franto, 2015**).

The interpretations presented herein are grounded in the findings of prior studies conducted in this area, which employed various surface and subsurface methodologies. The results obtained further substantiate the subsurface structural framework of northern Bangka, using high-resolution data and comprehensive investigative approaches.

5. Discussion

The delineation of subsurface structural settings through the utilization of satellite data, processed with techniques such as surface lineament extraction, enhanced edge detection (FSED), and Euler Deconvolution, produces optimal results that are mutually corroborative. This finding indicates that the lineament traces identified as geological features at the surface are indeed associated with subsurface structures formed during tectonic and deformation events in the northern Bangka Island region, specifically during the Palaeozoic and Mesozoic periods.

This study utilizes natural fracture measurements from granite rock outcrops, estimated to be of Triassic age, located in the Sungailiat area of northern Bangka, to validate the identified geological structures. **Figure 7a** illustrates the sites where these natural fracture measurements were taken. A total of six locations were assessed: Pantai Parai (G1 and G2), Pantai Rambak (G3 and G4), Pantai Batu Ketak (G5), and Pantai Mutiara Tikus (G6). Natural fractures measurements were conducted using the scanline method at each site, following the measurement approach depicted in **Figure 7b**. The measurement results indicate that the natural fractures observed in the granite outcrops exhibit distributions in various orientations, consistent with the regional structural patterns in the area. At locations G1 and G2, the natural fractures are predominantly aligned in the NE-SW and NW-SE directions. Additionally, location G2 exhibits an E-W orientation, which is hypothesized to have formed due to extensional processes.

At sites G3 and G4, in addition to the prevailing NW-SE and NE-SW orientations, a significant N-S direction is also observed, particularly at site G4. Similarly, at locations G5 and G6, the natural fractures primarily display NW-SE and NE-SW orientations. The observed variation in the orientations of natural fractures within the granitic rock outcrops throughout the study area is believed to be closely associated with the orientations of the predominant structural features. These results suggest that the development of natural fractures occurred concurrently with the formation of these regional structures.

Based on the findings from the literature review, as well as observations of natural fractures and the geological map of the study area, several tectonic events are identified that correlate with the formation of the primary structures in this region:

(1) NW-SE Trending Structures - These structures are associated with subduction and collision processes between continental plates (**Barber et al., 2005; Barber & Crow, 2009; Ko, 1986; Widana, 2013**). They correlate with the formation of parallel thrusts between the Pe-

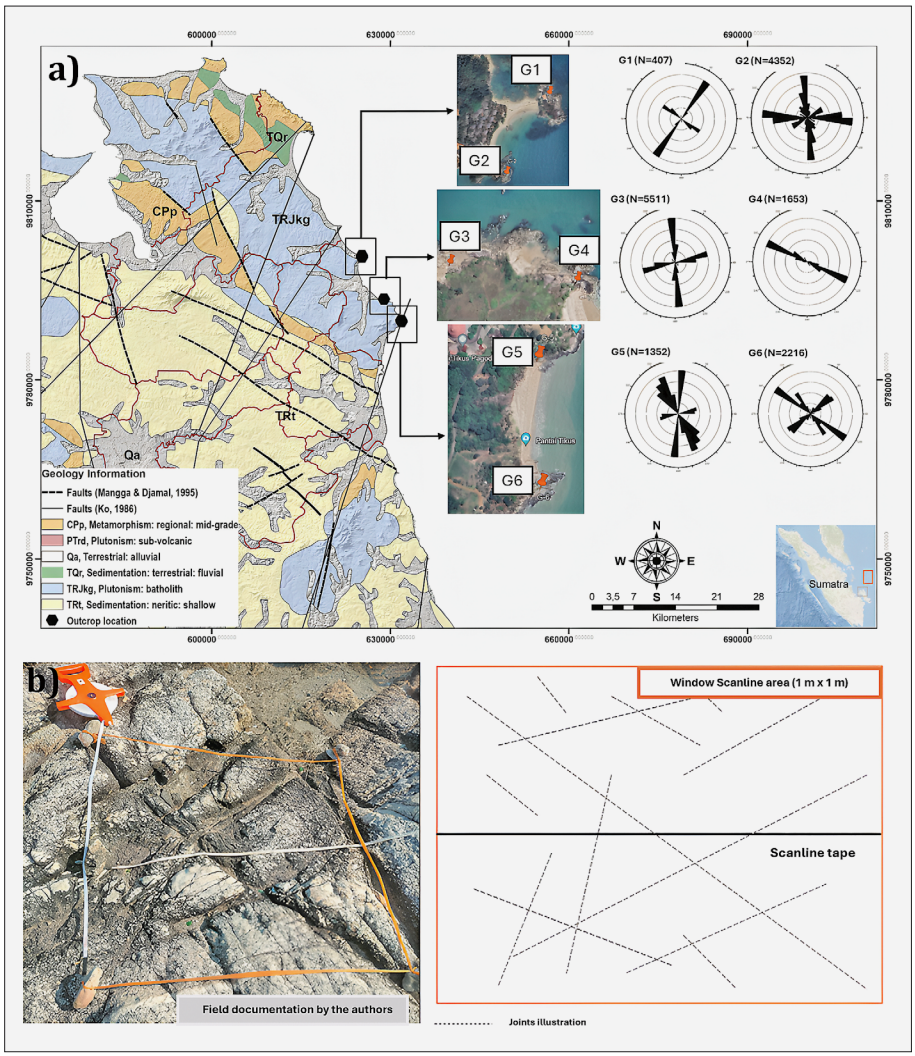

Figure 7. a) location map of measured natural fractures on granitic plutons outcrops; and **b)** the scanline method utilised in the study area

mali Formation and the Tanjung Genting Formation, both of which are aligned in the same NW-SE direction. This tectonic activity also initiated the intrusion of granite along an east-west direction during the Late Permian to Late Triassic period (**Ng et al., 2017; Wang et al., 2021**), mainly detected at location G2. The NW-SE trend is further interpreted to indicate lithological contacts in the northern Bangka region (**Franto, 2015**). Furthermore, the major east-west thrust juxtaposes folded Paleozoic and Triassic sequences, with granite intrusions aligned parallel to these faults, suggesting a genetic relationship (**Siregar et al., 2024**).

(2) the NE-SW trending regional shear faults. These represent tectonic events that have influenced the formation of shear faults, such as the Payung faults and the Pemali faults (**Anggraeni et al., 2023; Katili, 1967**). Subsequently, dextral, north-south-trending strike-slip systems dissected older thrusts and sedimentary packages, corresponding to Tertiary tectonic reactivation and basin subsidence (**Ko, 1986; Susilo et al., 2015**). It is strongly suspected that these faults have influenced the formation of fractures observed at locations G2, G3, and G5.

6. Conclusions

This study provides an in-depth examination of the fault structures beneath the surface of the Paleozoic-Mesozoic granitic basement of Bangka Island. The research utilized a multifaceted approach, incorporating surface lineament extraction, Fast-Sigmoid Edge Detection (FSED), and Euler Deconvolution. The analysis identified significant fault features trending NW-SE to E-W and NE-SW to N-S across various geological formations. These features are consistent with established regional tectonic patterns and indicate multiple phases of deformation.

We successfully identified concealed fault systems by applying FSED and Euler Deconvolution to gravity anomaly data. This methodology effectively delineates distinct rock layers and fractured zones at varying depths. Furthermore, comparing remote sensing data with field measurements of natural fractures within granitic outcrops corroborated the structural trends identified through analyses of satellite and gravity data. The findings of this study underscore the efficacy and cost-effectiveness of integrating high-resolution gravity data

with edge detection filters for analyzing subsurface structures, particularly in regions with limited geological exposure.

The results enhance our understanding of the tectonic framework in northern Bangka and provide a practical approach for identifying fractured basement reservoirs, which are crucial for hydrocarbon exploration in similar granitic environments.

Acknowledgement

The author wishes to express gratitude to several colleagues who contributed valuable insight and engaged in meaningful discussions related to this research. Their contributions have significantly enhanced the comprehensiveness of the interpretations presented in this paper.

Funding

This research is a component of a doctoral study being conducted at the Faculty of Geological Engineering at Padjadjaran University. It is being supported by the Indonesian Education Scholarship (BPI) in partnership with the Centre of Higher Education Financing and Assessment (PPAPT) and the Indonesian Endowment Fund for Education (LPDP) for the period from 2021 to 2025.

7. References

Ahmadi, H., & Pekkan, E. (2021). Fault-Based Geological Lineaments Extraction Using Remote Sensing and GIS – A Review. *Geosciences*, *11*(5), 183. https://doi.org/10.3390/geosciences11050183

Anggraeni, D., Siregar, R. N., & Sismanto, S. (2023). Identification of Subsurface Structures Using Topex Altimetry Satellite Gravity Data: Implications for Preliminary Surveys of Geothermal Existence. *International Journal of Hydrological and Environmental for Sustainability*, *2*(2), 88–96. https://doi.org/10.58524/ijhes.v2i2.261

Aprina, P. U., Santoso, D., Alawiyah, S., Prasetyo, N., & Ibrahim, K. (2024). Delineating geological structure utilizing integration of remote sensing and gravity data: a study from Halmahera, North Molucca, Indonesia. *Vietnam Journal of Earth Sciences*. https://doi.org/10.15625/2615-9783/20010

Areshev, E. G., Dong, T. Le, San, N. T., & Shnip, O. A. (1992). Reservoirs in fractured basement on the continental shelf of southern vietnam. *Journal of Petroleum Geology*, *15*(3), 451–464. https://doi.org/10.1111/j.1747-5457.1992.tb00719.x

Army, E. K., & Saepuloh, A. (2020). Field Verifications of Geological Structures Related to SAR Detected Lineaments. *IOP Conference Series: Earth and Environmental Science*, *417*(1). https://doi.org/10.1088/1755-1315/417/1/012012

Azman, A. I., Talib, J. A., & Sokiman, M. S. (2020). The Integration of Remote Sensing Data for Lineament Mapping in the Semanggol Formation, Northwest Peninsular Malaysia. *IOP Conference Series: Earth and Environmental Science*, *540*(1), 012026. https://doi.org/10.1088/1755-1315/540/1/012026

Barber, A. J., & Crow, M. J. (2009). Structure of Sumatra and its implications for the tectonic assembly of Southeast Asia and the destruction of Paleotethys. *Island Arc*, *18*(1), 3–20. https://doi.org/10.1111/j.1440-1738.2008.00631.x

Barber, A. J., Crow, M. J., & Milsom, J. S. (2005). Sumatra: Geology, Resources, and Tectonic Evolution. In *The Geological Society* (Geological). The Geological Society.

Bhardwaj, A., Jain, K., & Chatterjee, R. S. (2020). Refining IKONOS DEM for Dehradun Region Using Photogrammetry Based DEM Editing Methods, Orthoimage Generation and Quality Assessment of Cartosat-1 DEM. *IECG 2020*, 3. https://doi.org/10.3390/IECG2020-06966

Blakely, R. J. (1995). *Potential Theory in Gravity and Magnetic Applications*. Cambridge University Press.

Carvalho, R., & Batty, M. (2005). Encoding Geometric Information in Road Networks Extracted from Binary Images. *Environment and Planning B: Planning and Design*, *32*(2), 179–190. https://doi.org/10.1068/b31128c

Cobbing, E. J., Pitfield, P. E. J., Darbyshire, P. D. F., & Mallick, D. I. J. (1986). The granites of the Southeast Asian Tin Belt. *Journal of the Geological Society*, *143*, 537–550.

Cooper, G. (2008). Euler Deconvolution with Improved Accuracy and Multiple Different Structural Indices. *Journal of China University of Geosciences*, *19*(1), 72–76. https://doi.org/10.1016/S1002-0705(08)60026-6

Cuong, T. X., & Warren, J. K. (2009). Bach ho field, a fractured granitic basement reservoir, Cuu Long Basin, offshore SE Vietnam: A 'buried-hill' play. *Journal of Petroleum Geology*, *32*(2), pp 129-156. https://doi.org/10.1111/j.1747-5457.2009.00440.x

Echeverria, M. D. P. V., Ortega, A. G. V., Larreta, E., Romero Crespo, P., & Mulas, M. (2022). Lineament Extraction from Digital Terrain Derivate Model: A Case Study in the Girón–Santa Isabel Basin, South Ecuador. *Remote Sensing*, *14*(21), 5400. https://doi.org/10.3390/rs14215400

Eldosouky, A. M., Pham, L. T., Duong, V. H., Kemgang Ghomsi, F. E., & Henaish, A. (2022). Structural interpretation of potential field data using the enhancement techniques: a case study. *Geocarto International*, *37*(27), 16900–16925. https://doi.org/10.1080/10106049.2022.2120548

Enoh, M. A., Okeke, F. I., & Okeke, U. C. (2021). Automatic lineaments mapping and extraction in relationship to natural hydrocarbon seepage in Ugwueme, South-Eastern Nigeria. *Geodesy and Cartography (Vilnius)*, *47*(1), 34–44. https://doi.org/10.3846/gac.2021.12099

Farmakis-Serebryakova, M., & Hurni, L. (2020). Comparison of Relief Shading Techniques Applied to Landforms. *ISPRS International Journal of Geo-Information*, *9*(4), 253. https://doi.org/10.3390/ijgi9040253

Florinsky, I. V. (2016). Lineaments and Faults. *Digital Terrain Analysis in Soil Science and Geology*, 353–376. https://doi.org/10.1016/b978-0-12-804632-6.00014-6

Franto. (2015). Interpretasi Struktur Geologi Regional Pulau Bangka Berdasarkan Citra Shuttle Radar Topography Mis-

sion (SRTM) (Interpretation Structure of Regional Geology on Bangka Island with Shuttle Radar Topography Mission (SRTM)). *Jurnal Promine*, *3*(1), 10–20.

Ghosh, G. K. (2022). Study of gravity signature across the floating basement of Bundelkhand granite using 3D-Euler deconvolution, source edge detection technique and various gravity gradient analyses. *Acta Geophysica*, *70*(4), 1519–1537. https://doi.org/10.1007/s11600-022-00798-4

Gillespie, P. A., Holdsworth, R. E., Long, D., Williams, A., & Gutmanis, J. C. (2021). Introduction: geology of fractured reservoirs. *Journal of the Geological Society*, *178*(2). https://doi.org/10.1144/jgs2020-197

Gillespie, P., Gutmanis, J., Holdsworth, B., Long, D., Mcallister, E., Simon, S., Shell, P., Williams, A., Ameen, M. S., Aramco, S., Di Cuia, R., Laubach, S., & Trice, A. R. (2018, October). *The Geology of Fractured Reservoirs*. www.geolsoc.org.uk/petroleum

Gutmanis, J. (2009). Basement reservoirs - A review of their geological and production characteristics. *Society of Petroleum Engineers - International Petroleum Technology Conference 2009, IPTC 2009*, *1*, 358–364. https://doi.org/10.2523/iptc-13156-ms

Guttormsen, J. (2010). Naturally fractured basement reservoirs: using South Sumatra to characterize the challenges of exploring and exploiting fracture basement reservoirs. *Proc. Indon Petrol. Assoc., 34th Ann. Conv.*, *IPA10-G-18*(May 2010). https://doi.org/10.29118/IPA.742.10.G.183

Hall, R., Clements, B., & Smyth, H. R. (2009). Sundaland: Basement character, structure and plate tectonic development. *Proceedings, Indonesian Petroleum Association Thirty-Third Annual Convention & Exhibition*. https://www.researchgate.net/publication/268358722

Han, L., Liu, Z., Ning, Y., & Zhao, Z. (2018). Extraction and analysis of geological lineaments combining a DEM and remote sensing images from the northern Baoji loess area. *Advances in Space Research*, *62*(9), 2480–2493. https://doi.org/10.1016/j.asr.2018.07.030

Hendrawan, R., Draniswari, W. A., Wahyuni, F. I., Sapiie, B., & Basuki, N. I. (2024). Metamorphic Complex Deformation in North Bangka Island Based on Macrostructures and Microstructures Evidences. *Journal of Geoscience, Engineering, Environment, and Technology*, *9*(2), 134–139. https://doi.org/10.25299/jgeet.2024.9.2.13379

Hennings, P., Allwardt, P., Paul, P., Zahm, C., Reid, R., Alley, H., Kirschner, R., Lee, B., & Hough, E. (2012). Relationship between fractures, fault zones, stress, and reservoir productivity in the Suban gas field, Sumatra, Indonesia. *AAPG Bulletin*, *96*(4), 753–772. https://doi.org/10.1306/08161109084

Hirt, C. (2014). Digital Terrain Models. In *Encyclopedia of Geodesy* (pp. 1–6). Springer International Publishing. https://doi.org/10.1007/978-3-319-02370-0_31-1

Hirt, C., Claessens, S., Fecher, T., Kuhn, M., Pail, R., & Rexer, M. (2013). New ultrahigh-resolution picture of Earth's gravity field. *Geophysical Research Letters*, *40*(16), 4279–4283. https://doi.org/10.1002/grl.50838

Hobbs, W. H. (1904). Lineaments of the Atlantic Border region. *Bulletin of the Geological Society of America*, *15*, 483–506. https://doi.org/10.1130/GSAB-15-483

Hung, N. Du, Le, H. Van, Joc, H. V., & Minh, H. C. (2003). Hydrocarbon Geology of Cuu Long Basin - Offshore Vietnam. *AAPG; Search and Discovery*, *1*(1), 21–24.

Hung, L. Q., Batelaan, O., & De Smedt, F. (2005). Lineament extraction and analysis, comparison of LANDSAT ETM and ASTER imagery. Case study: Suoimuoi tropical karst catchment, Vietnam. In M. Ehlers & U. Michel (Eds.), *Remote Sensing for Environmental Monitoring, GIS Applications, and Geology V* (Vol. 5983, p. 59830T). SPIE. https://doi.org/10.1117/12.627699

Hung, N., & Le, H. (2004). Petroleum Geology of Cuu Long Basin - Offshore Vietnam. *American Association of Petroleum Geologists. Search and Discovery, Article #10062.*

Hutchison, C. S. (2014). Tectonic evolution of Southeast Asia. *Bulletin of the Geological Society of Malaysia*, *60*(December), 1–18. https://doi.org/10.7186/bgsm60201401

Kamto, P. G., Oksum, E., Yap, L., Kande, L. H., & Kamguia, J. (2023). High precision structural mapping using advanced gravity processing methods: a case study from the North region of Cameroon. *Acta Geophysica*. https://doi.org/10.1007/s11600-023-01211-4

Katili, J. A. (1967). Structure and Age of The Indonesian Tin Belt with Special Reference to Bangka. *Tectonophysics*.

Katili, J. A. (1972, June). Plate tectonics of Indonesia with special reference to the Sundaland area. *Proceedings Indonesian Petroleum Association First Annual Convention*.

Ko, U. (1986). Preliminary synthesis of the geology of Bangka Island, Indonesia. In *Bulletin of the Geological Society of Malaysia* (Vol. 1).

Koning, T., Cameron, N., & Clure, J. (2021). Undiscovered Potential in the Basement Exploring in Sumatra for oil and gas in naturally fractured and weathered basement reservoirs. *Berita Sedimentologi*, *47*(2), 67–79. https://doi.org/10.51835/bsed.2021.47.2.320

Kumar, R., & Singh, K. A. (2021). Delineation of subsurface features by gravity technique in parts of Shivpuri District, M.P. *MAUSAM*, *72*(3), 661–668. https://doi.org/10.54302/mausam.v72i3.1316

Kumar, U., Pal, S. K., Sahoo, S. D., Narayan, S., Saurabh, Mondal, S., & Ganguli, S. S. (2018). Lineament Mapping over Sir Creek Offshore and its Surroundings using High Resolution EGM2008 Gravity Data: An Integrated Derivative Approach. *Journal of the Geological Society of India*, *91*(6), 671–678. https://doi.org/10.1007/s12594-018-0922-x

Kurniawan, B. A. (2018). Application of 3D Seismic Volume Curvature for Basement Fracture Delineation, Case Study : Suban Field, South Sumatra Basin. *Proc. Indon Petrol. Assoc., 36th Ann. Conv.*, *C*(May). https://doi.org/10.29118/IPA.0.12.G.170

Li, B., Guttormsen, J., Hoi, T., & Duc, N. (2004). Characterizing Permeability for the Fractured Basement Reservoirs. *Proceedings of SPE Asia Pacific Oil and Gas Conference and Exhibition*, *October 2004*, 271–281. https://doi.org/10.2523/88478-MS

Li, L., Huang, D., Han, L., & Ma, G. (2014). Optimised edge detection filters in the interpretation of potential field data.

Exploration Geophysics, *45*(3), 171–176. https://doi.org/10.1071/EG13059

Liu, J., Li, S., Jiang, S., Wang, X., & Zhang, J. (2023). Tools for Edge Detection of Gravity Data: Comparison and Application to Tectonic Boundary Mapping in the Molucca Sea. *Surveys in Geophysics*, *44*(6), 1781–1810. https://doi.org/10.1007/s10712-023-09784-x

Ma, G., Liu, C., & Li, L. (2014). Balanced horizontal derivative of potential field data to recognize the edges and estimate location parameters of the source. *Journal of Applied Geophysics*, *108*, 12–18. https://doi.org/10.1016/j.jappgeo.2014.06.005

Mangga, A. A., & Djamal, B. (1994). *Peta Geologi Lembar Bangka Utara, Sumatera (Skala 1:250.000)*.

Margono, U., Supandjono, R., & Partoyo, E. (1995). *Geological Map of the South Bangka Sheet, Sumatera*.

McCourt, W. J., Crow, M. J., Cobbing, E. J., & Amin, T. C. (1996). Mesozoic and Cenozoic plutonic evolution of SE Asia: evidence from Sumatra, Indonesia. *Geological Society, London, Special Publications*, *106*(1), 321–335. https://doi.org/10.1144/GSL.SP.1996.106.01.21

Melo, F. F., & Barbosa, V. C. F. (2018). Correct structural index in Euler deconvolution via base-level estimates. *GEOPHYSICS*, *83*(6), J87–J98. https://doi.org/10.1190/geo2017-0774.1

Melouah, O., & Pham, L. T. (2021). An improved ILTHG method for edge enhancement of geological structures: application to gravity data from the Oued Righ valley. *Journal of African Earth Sciences*, *177*, 104162. https://doi.org/10.1016/j.jafrearsci.2021.104162

Metcalfe, I. (2000). The Bentong-Raub Suture Zone. *Journal of Asian Earth Sciences*, *18*(6), 691–712. https://doi.org/10.1016/S1367-9120(00)00043-2

Metcalfe, I. (2013). Tectonic evolution of the Malay Peninsula. *Journal of Asian Earth Sciences*, *76*, 195–213. https://doi.org/10.1016/j.jseaes.2012.12.011

Metcalfe, I. (2017). Tectonic evolution of Sundaland. *Bulletin of the Geological Society of Malaysia*, *63*(November), 27–60. https://doi.org/10.7186/bgsm63201702

Mohammed, A., K, P., Kumanan, C. J., & Ramasamy, SM. (2010). Significance of Surface Lineaments for Gas and Oil Exploration in Part of Sabatayn Basin-Yemen. *Journal of Geography and Geology*, *2*(1), 119–128. https://doi.org/10.5539/jgg.v2n1p119

Narr, W., Schechter, D. S., & Thompson, L. B. (2006). Naturally Fractured Reservoir Characterization. In *Society of Petroleum Engineers*. Society of Petroleum Engineers.

Nasuti, Y., Nasuti, A., & Moghadas, D. (2019). STDR: A Novel Approach for Enhancing and Edge Detection of Potential Field Data. *Pure and Applied Geophysics*, *176*(2), 827–841. https://doi.org/10.1007/s00024-018-2016-5

Ng, H.-F. (2006). Automatic thresholding for defect detection. *Pattern Recognition Letters*, *27*(14), 1644–1649. https://doi.org/10.1016/j.patrec.2006.03.009

Ng, S. W.-P., Whitehouse, M. J., Roselee, M. H., Teschner, C., Murtadha, S., Oliver, G. J. H., Ghani, A. A., & Chang, S.-C. (2017). Late Triassic granites from Bangka, Indonesia: A continuation of the Main Range granite province of the South-East Asian Tin Belt. *Journal of Asian Earth Sciences*, *138*, 548–561. https://doi.org/10.1016/j.jseaes.2017.03.002

Ni, C., Zhang, S., Liu, C., Yan, Y., & Li, Y. (2016). Lineament Length and Density Analyses Based on the Segment Tracing Algorithm: A Case Study of the Gaosong Field in Gejiu Tin Mine, China. *Mathematical Problems in Engineering*, *2016*, 1–7. https://doi.org/10.1155/2016/5392453

Oksum, E., Le, D. V., Vu, M. D., Nguyen, T. H. T., & Pham, L. T. (2021). A novel approach based on the fast sigmoid function for interpretation of potential field data. *Bulletin of Geophysics and Oceanography*, *62*(3), 543–556. https://doi.org/10.4430/bgta0348

P'an, C.-H. (1982). Petroleum in Basement Rocks. *American Association of Petroleum Geologists Bulletin*, *66*(10), 1597–1643. https://doi.org/10.1306/03b5a994-16d1-11d7-8645000102c1865d

Permana, B. R., Yusim, S., Darmadi, Y., & Firdaus, M. (2023). Integration of core analysis, logs, seismic and dynamic data in defining fracture reservoir: case study suban field, south sumatra. *Proceedings, Indonesian Petroleum Association Forty-Seventh Annual Convention & Exhibition*. https://www.researchgate.net/publication/372689625

Petford, N., & McCaffrey, K. (2003). Hydrocarbons in crystalline rocks: An introduction. *Geological Society Special Publication*, *214*(2002), 1–5. https://doi.org/10.1144/GSL.SP.2003.214.01.01

Pham, L. T. (2024). An improved edge detector for interpreting potential field data. *Earth Science Informatics*, *17*(3), 2763–2774. https://doi.org/10.1007/s12145-024-01286-7

Pham, L. T., Eldosouky, A. M., Melouah, O., Abdelrahman, K., Alzahrani, H., Oliveira, S. P., & Andráš, P. (2021). Mapping subsurface structural lineaments using the edge filters of gravity data. *Journal of King Saud University - Science*, *33*(8), 101594. https://doi.org/10.1016/j.jksus.2021.101594

Pham, L. T., Ghomsi, F. E. K., Vu, T. Van, Oksum, E., Steffen, R., & Tenzer, R. (2023). Mapping the structural configuration of the western Gulf of Guinea using advanced gravity interpretation methods. *Physics and Chemistry of the Earth, Parts A/B/C*, *129*, 103341. https://doi.org/10.1016/j.pce.2022.103341

Pham, L. T., Oliveira, S. P., Abdelrahman, K., Gomez-Ortiz, D., Nguyen, D. V., Vo, Q. T., & Eldosouky, A. M. (2024). Selection of Euler deconvolution solutions using the enhanced horizontal gradient and stable vertical differentiation. *Open Geosciences*, *16*(1). https://doi.org/10.1515/geo-2022-0637

Prabowo, I. A., Verdiansyah, O., & Prabowo, R. (2021). *Extraction of Lineament Density Analysis from ASTER DEM for Determine the Vein Direction*. *Figure 1*. https://doi.org/10.4108/eai.30-8-2021.2311530

Reid, A., Geophysics, R., of Leeds, U., FitzGerald, D., & McInerny, P. (2003). Euler deconvolution of gravity data. *SEG Annual Meeting, Dallas, Texas, October 2003*. https://doi.org/http://dx.doi.org/10.13140/2.1.3210.0489

Reid, A., Geophysics, R., & Thurston, J. (2012). The Structural Index in gravity and magnetic interpretation: errors, uses

and abuses. *SEG Technical Program Expanded Abstracts 2012*, 1–6. https://doi.org/10.1190/segam2012-0152.1

Rusinkiewicz, S., Burns, M., & DeCarlo, D. (2006). Exaggerated shading for depicting shape and detail. *ACM Transactions on Graphics*, *25*(3), 1199–1205. https://doi.org/10.1145/1141911.1142015

Safani, J., IBRAHIM, K., DENI, W., RUBAIYN, A., FIRDAUS, F., & HARISMA, H. (2023). Interpreting structural configuration of the Sengkang Basin of Indonesia using edge detection and 3-D Euler deconvolution to satellite gravity data. *Turkish Journal of Earth Sciences*, *32*(7), 894–914. https://doi.org/10.55730/1300-0985.1881

Salui, C. L. (2018). Methodological Validation for Automated Lineament Extraction by LINE Method in PCI Geomatica and MATLAB based Hough Transformation. *Journal of the Geological Society of India*, *92*(3), 321–328. https://doi.org/10.1007/s12594-018-1015-6

Schultz, A. (2014). Satellite Interferometry and the Detection of Active Deformation Associated With Faults in Suban Field, South Sumatra Basin, Indonesia. *Proc. Indonesian Petrol. Assoc., 38th Ann. Conv.*, *May*. https://doi.org/10.29118/IPA.0.14.G.068

Sembiring, D. K., Indriana, R. D., & Yulianto, T. (2023). Subsurface Model Of Mt. Sinabung Using The GGM-Plus Satellite Gravity Data And Deconvolution Euler. *International Journal of Progressive Sciences and Technologies*, *39*(1), 169–176.

Siregar, R. N., Nukman, M., Widana, K. S., Harijoko, A., & Sismanto, S. (2024). Radiogenic geothermal systems of Bangka Island, Indonesia: Implications of high heat production and tectonic framework. *Energy Geoscience*, *5*(4), 100306. https://doi.org/10.1016/j.engeos.2024.100306

Soleha, K. P., Handyarso, A., Fitriani, D., & Supriyana, E. (2019). Modeling of subsurface based on gravity data with second vertical derivative (SVD) and Euler deconvolution optimization. *IOP Conference Series: Earth and Environmental Science*, *311*(1), 012065. https://doi.org/10.1088/1755-1315/311/1/012065

Spector, A., & Grant, F. S. (1970). Statistical models for interpreting aeromagnetic data. *Geophysics*, *35*(2), 293–302. https://doi.org/10.1190/1.1440092

Susilo, Y. S., Anzhar, K., Sastratenaya, S., Godoy, A. R., & Serva, L. (2015). SEISMOTECTONIC CONSIDERATIONS ON BANGKA ISLAND NPP SITING. *Prosiding Seminar Nasional Teknologi Energi Nuklir*.

Suyoto, H. (2010). A fractured pre-tertiary Basement Reservoir Engineering Study. *Proc. Indon Petrol. Assoc., 34th Ann. Conv.*, *May 2010*. https://doi.org/10.29118/IPA.1409.10.E.064

Tjia, H. D. (2007). Fractured Granitic Basement as Reservoir. *Proceedings joint convention bali. The 32th HAGI, the 36th IAGI, and the 29th IATMI Annual Conference and Exhibition*, 1414–1417.

Van Gorsel, J. T. (2018). Bibliography of the geology of Indonesia and surrounding areas - PART II. Sumatra-Sundaland (Sumatra, 'Tin Islands', Sunda Shelf, Natuna). *Bibiliography of Indonesian Geology*, *7.0*, 0–315. http://www.vangorselslist.com/pdf/BIG_I_Regional_7.pdf

Vincent, O., & Folorunso, O. (2009). *A Descriptive Algorithm for Sobel Image Edge Detection*. https://doi.org/10.28945/3351

Wang, Y., Qian, X., Zhang, Y., Gan, C., Zhang, A., Zhang, F., Feng, Q., Cawood, P. A., & Zhang, P. (2021). Southern extension of the Paleotethyan zone in SE Asia: Evidence from the Permo-Triassic granitoids in Malaysia and West Indonesia. *Lithos*, *398–399*. https://doi.org/10.1016/j.lithos.2021.106336

Widana, K. S. (2013). Petrografi dan Geokimia Unsur Utama Granitoid Pulau Bangka: Kajian Awal Tektonomagmatisme. *Eksplorium*, *34*, 1–16. https://www.researchgate.net/publication/318642660

Yao, Y., Huang, D., Yu, X., & Chai, B. (2016). Edge interpretation of potential field data with the normalized enhanced analytic signal. *Acta Geodaetica et Geophysica*, *51*(1), 125–136. https://doi.org/10.1007/s40328-015-0120-x

Bampourda, D., Argialas, D., Nomikou, P., & Tzotsos, A. (2017). An object-based image analysis approach for the extraction of the Kolokthron volcano and associated domes-cones from a digital seabed elevation model. *Bulletin of the Geological Society of Greece*, *50*(3), 1616. https://doi.org/10.12681/bgsg.11881

SAŽETAK

Integrirana analiza rasjeda temeljnoga sloja na otoku Bangka u Indoneziji korištenjem gustoće površinskih lineamenata i pojačanja gravitacijskih anomalija

Otok Bangka nastao je subdukcijom i sudarom blokova Sibumasu i Istočna Malaja, koji su potekli iz Gondvane, u kasnome paleozoiku. Njegovu sjevernu regiju čine permske metamorfne stijene kompleksa Pemali, trijaske sedimentne jedinice formacije Tanjunggenting te graniti formacije Klabat iz kasnoga trijasa do rane jure. Unatoč višestrukim tektonskim fazama koje su oblikovale otok Bangka strukturna konfiguracija rasjeda i nabora u podlozi u sjevernoj regiji ostaje slabo razjašnjena. Ova neizvjesnost otežava procjenu ležišta u rasjednom temeljnom sloju u području istraživanja. Kako bi se popunila ova praznina, ova studija integrira ekstrakciju površinskih lineamenata iz DEMNAS-a s podatcima o gravitacijskim anomalijama iz GGMplus-a kako bi se istražila struktura rasjeda temeljnog sloja sjeverne Bangke. Brza detekcija rubova sigmoidom (FSED) i Eulerova dekonvolucija primijenjene su za poboljšanje strukturne interpretacije i procjenu dubine podloge. Dominantne strukturne orijentacije sjeverozapad-jugoistok i sjeveroistok-jugozapad identificirane na površini bile su u skladu s podzemnim značajkama, dok su FSED i Eulerova dekonvolucija također otkrile trendove istok-zapad i sjever-jug. Štoviše, rezultati Eulerove dekonvolucije uputili su na dubine temeljnoga sloja od 3000 do 4000 m ispod razine mora. Mjerenja pukotina na terenu iz granitnih izdanaka potvrđuju ove orijentacije, naglašavajući snažnu podudarnost između površinskih i podzemnih struktura. Ovi nalazi pružaju nove uvide u tektonsku evoluciju sjeverne regije otoka Bangka i ističu orijentacije rasjeda koje bi mogle poslužiti kao smjernice za identifikaciju zona rasjednih ležišta u granitnim terenima.

Ključne riječi:
gustoća linije, poboljšana detekcija rubova, gravitacijska anomalija, strukture rasjeda temeljnog sloja, otok Bangka

Author's contribution

Harnanti Yogaputri Hutami (Ms.): conceptualisation, investigation, formal analysis, validation, and writing – the original draft. **Erlangga Ibrahim Fattah** and **Nugroho Prasetyo** (Mr.): data curation in FSED and Euler Deconvolution methodologies, visualisation, and formal analysis. **Nur Ayu Anas** (Ms.): data curation in lineament extraction and lineament density methodologies, formal analysis, visualisation, and writing – the original draft. **Edy Sunardi and Iyan Haryanto** (Professor): the supervisor team and validation. **Sonny Winardhi** (PhD): supervisor team, formal analysis, and validation.
All authors have read and agreed to the published version of the manuscript.